Available online at www.sciencedirect.com
SCIENCE DIRECT®
Journal of Power Sources 131 (2004) 304–312
JOURNAL OF POWER SOURCES
www.elsevier.com/locate/jpowsour

Generalized model of planar SOFC repeat element for design optimization

D. Larrain*, J. Van herle, F. Maréchal, D. Favrat

Laboratory for Industrial Energy Systems (LENI), Faculty of Engineering, Swiss Federal Institute of Technology, Lausanne 1015, Switzerland

Received 30 September 2003; accepted 6 November 2003

Abstract

A model for planar solid oxide fuel cell repeat elements and stacks has been developed. Distribution of concentrations, reaction rates and temperatures (both gases and solids) are computed as well as overall performance results. Specific experiments provide inputs to the model by a parameter estimation method.

The modeling approach developed allows to compare several configurations. As the number of design parameters is large (from cell size, component thicknesses to gas flow configuration), the model is designed to change easily these parameters so as to explore as many cases as possible. This is particularly true for the flow configuration (inlet position, outlets) for which several options are considered.

This model assists in choosing a configuration and allows to perform sensitivity studies in an efficient way (without having to produce a new mesh such as for CFD tools) or to be combined with an optimization tool. A first validation with experimental results, performed on a particular stack design, is presented. Issues of model accuracy and sensitivity to uncertain inputs are discussed.

Keywords: SOFC; Model; Repeat element; Validation

1. Introduction

Design and development of a solid oxide fuel cell stack is a task involving many different aspects. The goals for a stack can be very challenging: maximum power output, compactness and long term stability. The trend to increase power densities may be in contradiction with degradation behavior, the drawback being an increased temperature and gradient, which is likely to induce accelerated degradation and failure. On the other side, constraints from the system (such as the maximum pressure drop on the stack), ceramic fabrication feasibility and cost aspects add more elements to consider.

Modeling can be a tool to help decision making on some important stack characteristics. Several models are published in literature [1–3]. These models represent a particular defined configuration.

This work is being realized in the frame of a stack development project. The focus and aim of the model developed is to be able to compare different configuration, explore geometrical parameters and predict performance and behavior of the existing repeat element and stacks.

The complete mathematical description is based on the following equations: conservation of momentum with a porous media description, conservation of species for both gases (expressed in moles), conservation of energy for gases, conservation of energy for the solid (assumed as monolithic).

This work assumes that a 2D model, combined with optimization, will allow to identify better configurations, optimize the decision variables and reduce the number of experiments in the development process. In the different levels of details for stack modeling, CFD models are accurate with a good geometry definition and complete solving of transport phenomena, on the other hand, a 1D model would not allow to capture the behavior of the considered configuration. The gap between these two model types has to be filled in, as CFD is not an efficient tool to explore new geometry and optimize design parameters: the mesh generation is a long process and CPU time for simulation is long. The presented model aims to provide the essential information from a CFD model (such as velocity, pressure,

* Corresponding author. Tel.: + 41-21-693-53-57; fax: +41-21-693-35-02.
E-mail address: diego.larrain@epfl.ch (D. Larrain).

0378-7753/$ – see front matter © 2004 Elsevier B.V. All rights reserved.
doi:10.1016/j.jpowsour.2003.11.088

concentration and temperature field) with a more efficient computing time and flexibility.

Equations and assumptions made in the model are presented, then important inputs and results obtained are shown. Accuracy issues are discussed. As the model needs to be validated experimentally to be used as a decision tool, some elements of validation are presented. Finally, an example of comparison of configurations is presented.

2. The repeat element configuration

The repeat element considered is based on an anode supported cell and metallic interconnects and is designed to operate around 1050 K. This concept has demonstrated an electrical output, 100 We with a stack of six cells (of 52 cm^2 active area per cell). One of the main features of this stack is to used internal manifolding feed the reactants to the cell, therefore no additional pieces are needed and the stack is very compact. The inlet of gases is punctual and the outlet is distributed on a side. The current lines of the flow field are therefore in 2D (see in Fig. 1a). On most of the cell surface, the flow is approximately in counter flow mode.

The current repeat element uses square cells of 80 mm side, the active surface (accounting for the surface occupied by sealing and border) is of ca. 52 cm^2. The total repeat element thickness is below 3 mm with a 250 μm thick cell (200 μm for the anode support, 6 μm thin electrolyte and ca. 50 μm porous cathode), interconnects of 0.75 mm and gas diffusion layers of 0.5 mm on both sides.

From the experimental side, the different dimensions are fixed. In a design mode, however, the degrees of freedom are: the cell total area and geometry (length, aspect ratio), the inlet position, the gas diffusion layer and interconnect thickness. These geometrical decision variables are linked to the operating variables such as the fuel and air flow rates (under the constraint of pressure drop targets for the repeat element).

Based on the same technology using internal manifolding, other configurations are possible, one example is a case with a central feed of hydrogen and two inlets for the air flow which represented in Fig. 1(b). A comparison of these two configurations is presented in Section 6.

3. Model

The repeat element configurations considered are in obvious need for 2D modeling. The fluid patterns cannot be represented by simple mono-dimensional flow. The geometric definition of the model is presented in Fig. 1(c) for the present configuration. As the cell design is symmetric (with an axes passing through the inlets), only half of the cell have been modeled. The lengths of the cell are variables of the model, the inlet coordinates are parameters of the model.

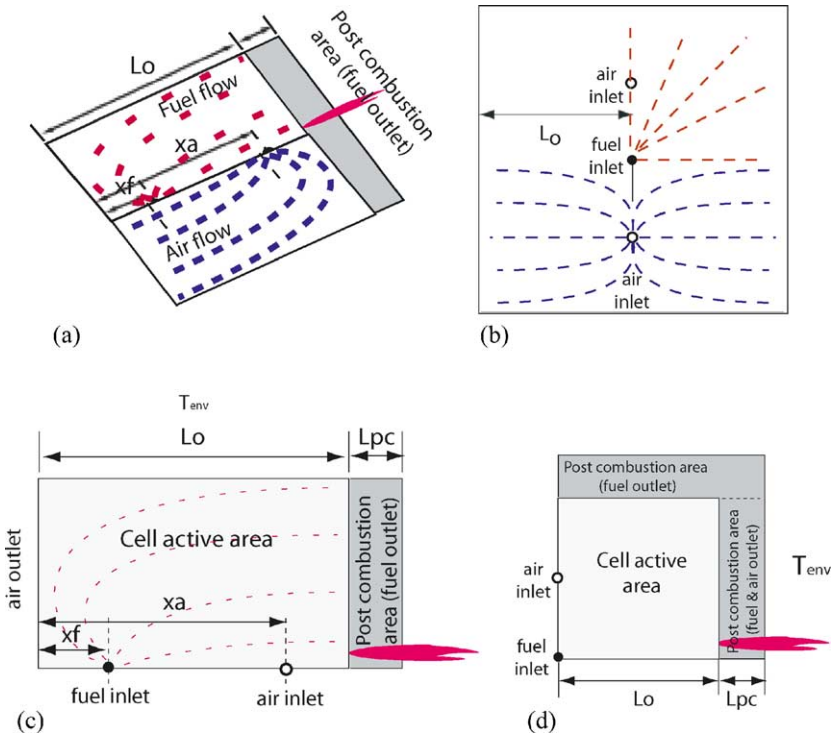

Fig. 1. Configuration simulated and geometrical models. (a) Configuration "counter flow," (b) configuration central feed, (c) model for "counter flow" geometry, (d) model for central feed geometry.

In Fig. 1(d), two axes of symmetry (one passing by the three inlets, and the other one by the central inlet) allow to model only a quarter of the cell. The following section presents the assumptions and equations used in the model.

3.1. Fluid flow and species balance

The fluid pattern in the gas diffusion layer is a 3D phenomenon with 2D streamlines and a velocity profile in the height of the channel. The model developed assumes a plug flow in the height of the channel to reduce the flow description to a 2D flow pattern, which is the main feature of this repeat element model.

To describe the fluid flow and species balance equations, several options are possible. The main assumptions made here are: the total molar concentration of species is decoupled from the temperature field, the change in total number of moles is decoupled from the velocity field, and the viscosity of the fluid is assumed constant as well. These three assumptions decouple the fluid motion from the energy equations and the species balance. The essential coupling of the reaction rate with the species concentration and temperature is made by the kinetic model used. Solving the complete set of equations for the momentum, species balance and energy requires a CFD tool using a finite volume method for the resolution which is not the goal of the present work.

If no reforming is considered (operation with hydrogen) the total number of moles is constant on the fuel side. However, on the air side the number of species decreases: considering for example an air ratio of 2 and 70% fuel utilization, the oxygen utilization is 35% and the total number of moles decreases by ca. 8%. Then the error on the velocity field for the air side is of ca. 8%. The decoupling from the temperature causes the same amount of error to the velocity field with a maximum temperature difference of 100 K (which is quite common in SOFC). Nevertheless, as the species balance is expressed in terms of molar flux, this assumption does not affect the consistency of the species balance. The main error expected is on the pressure drop estimation which does not account for the acceleration of the fluid neither for the change in viscosity.

The presented assumptions lead to the following equation system. For the fluid flow, the velocity is linked to the pressure field by a Darcy equation in 2D.

$$-\vec{\nabla}(P) = \frac{\mu}{K}\vec{v} \tag{1}$$

where $\vec{v}$ is the velocity vector on x and y; μ is the dynamic viscosity; P is the pressure; K is the permeability coefficient determined experimentally.

Since the total mole change is assumed zero and the viscosity constant, the pressure field is computed from the boundary conditions with a Laplace equation

$$\Delta P = 0 \tag{2}$$

Finally, the species balance is therefore computed with an equation including convective and diffusive transport:

$$\vec{\nabla} \cdot \vec{F}_i - D\Delta \mathcal{C}_i = \dot{r}_i \tag{3}$$

where $\vec{F}_i$ is the local molar flux vector (on x and y direction) of species i; $\dot{r}_i$ is the rate of reaction per unit volume; D is the binary diffusion coefficient computed from the Fuller–Schettler–Giddings equation [4].

The boundary conditions applied on the fluid equations are:

- inlet concentration fixed at inlet
- uniform pressure at the outlet
- as the punctual inlet is a mathematical singularity (infinite velocities), the rate of reaction and the velocity are fixed to zero at the inlet
- the wall boundary condition is defined setting the velocity vector component normal to the wall to zero, and the diffusive term $(\partial \mathcal{C}_i/\partial n) = 0$.
- as post-combustion is included in the model, the domain modeling the fuel flow is extended to a post-combustion area where an almost complete combustion of hydrogen is assumed at the outlet of the domain.

3.2. Energy equations

Energy equations are defined for the solid part, assuming averaged thermal properties [1,2,5,6]. The method used for volume averaging here is a simple connexion of series and parallel conduction [7,8], the thermal transport properties are considered as isotropic. The solid energy equation is therefore:

$$\lambda_{s_{x,y}}\left(\frac{\partial^2 T_{\text{solid}}}{\partial x^2} + \frac{\partial^2 T_{\text{solid}}}{\partial y^2}\right) + \dot{Q} = 0 \tag{4}$$

where $\lambda_{s_{x,y}}$ is the average thermal conductivity, $\dot{Q}$ is the sum of the volumetric sources including the heat from the electrochemical reaction, the electric power removed from the system and heat transfer to the fluids. For the fluids, the energy equation is a local enthalpy balance:

$$\sum_{i=1}^{n_{\text{comp}}} \mathcal{C}_{p_i}\left(F_{i-x}\frac{\partial T_{\text{gas}}}{\partial x} + F_{i-y}\frac{\partial T_{\text{gas}}}{\partial y}\right) = \dot{Q} \tag{5}$$

where $\mathcal{C}_{p_i}$ is the heat capacity of species i; F_{i-x} is the local molar flux of i in the x direction; and $\dot{Q}$ is the volumetric heat sources which are essentially the heat transfer with the solid and the enthalpy of reactants and products.

3.3. Kinetics

As the model represents a repeat element based on anode supported cells, the current path through the electrolyte is assumed to be normal to the surface and the equation for the conservation of charge is not solved. The local reaction rate is computed with the following scheme:

$$U_{\text{cell}} = U_{\text{Nernst}} - R_{\text{ohmic}} \times j - \eta_{\text{act}} \tag{6}$$

where U_{Nernst} is the Nernst potential computed locally from the temperature and the partial pressures; U_{cell} is the cell operating voltage; j is the local current density; and η_{act} is the sum of overpotentials. The local resistance and activation overpotential are functions of temperature and current density.

3.4. Implementation of the model

The set of equation described has been implemented in the gPROMS tool which is an equation solver based tool allowing to solve distributed domains [9]. The scheme used to solve the distributed domain is centered finite difference. This tool have embedded parameter estimation and optimization solvers. As this tool is based on a equation solver, it gives the possibility to change the input variables and degrees of freedom of the problem.

The presented equations have been implemented in a normalized form allowing efficient sensitivity on the shape and size of the cell.

4. Model outputs and validation

The results from the implemented model are dependent on the boundary conditions applied and the input variables used for some properties. The outputs of the model are presented and validation of the model consistency with the mesh size is discussed.

4.1. Thermal boundary conditions applied

Boundary conditions applied to the model are essential as they affect the temperature field. Usually repeat element are assumed to be in the middle of a stack with adiabatic boundary condition. This boundary condition is easily defined. However, previous work [1,10] shows that for a stack mounted with metallic interconnects, no adiabatic cells are found. Adiabatic conditions are then the worst case scenario, but do not represent the reality for short stacks. The results for the IV characteristics presented are simulated with heat flux to the environment to represent a single repeat element test.

Post-combustion is considered in the model. To compute this contribution, the enthalpy of combustion of the remaining species of hydrogen is computed on each point of the fuel outlet (see in Fig. 1(c)) [2]. However, one of the uncertainties on the post-combustion contribution is the proportion of heat which is really absorbed by the repeat element, this depends on where the post-combustion flame is located. This flame starts on the border of the stack but extends to the environment. Therefore, it is assumed that part of the heat only is absorbed by the stack.

4.2. Model inputs

The equations defined in Section 3 need some input variables to be defined. When available, experimental data is used, however some values are known and found in the literature. Some of these inputs are uncertain and the response has to be evaluated.

The heat conduction of the cell is computed from the value for the anode cermet [11], electrolyte and cathode. The cermet is assumed to have 40% volume Ni and 50% porosity. Recent values for perovskites materials (cathode) are difficult to find [12].

The heat transfer coefficient is computed from a Nusselt number for laminar flow between parallel plates (≈ 8) and the exchange surface takes into account the surface added by the current collector. Some uncertainties remain on the heat transfer coefficient, especially when considering that the surface layers of the cell are porous, but the model is not very sensitive to this parameter (for Nusselt numbers in the range of 8–20, the magnitude of the temperature response differs by 10 K at the maximum temperature point).

Another uncertainty is the proportion of heat from the post-combustion which is absorbed by the stack. However, it has a small incidence on the performance and temperature results if varied in the range 0.25–0.75.

For the radiative boundary condition, the emissivity is assumed to be at 0.9. But again, varying this parameter between 0.7 and 0.9 has not a major influence on the results.

The input values for the kinetic parameters are obtained by a parameter identification method from experimental results on a button cell of 1 cm^2 active area [13]. The contribution of the interface resistance between current collectors and interconnects are taken from experiments [14] (Table 1) .

The lengths of the cell edges are variables and therefore sensitivity to the cell size and to the aspect ratio can easily be performed.

The decision variables have been listed in Section 2.

4.3. Model outputs

The model computes fields of pressure, velocity, concentration, reaction rates and temperature. Fig. 2 shows the concentration field for hydrogen and solid temperature. From Fig. 2(b), it can be noticed that punctual inlet induces large regions with lean fuel concentration. At the outlet, the concentration profile is not homogeneous, with higher

Table 1
Input variables for the model

Input	Units	Range
Cermet conductivity	W/mK	8.9
Interconnect conductivity	W/mK	25 (@1100 K)
Fraction heat post-combustion	–	0.25–0.75 (**0.5**)
Emissivity	–	0.9
Nusselt number (two plates)	–	≈ 8

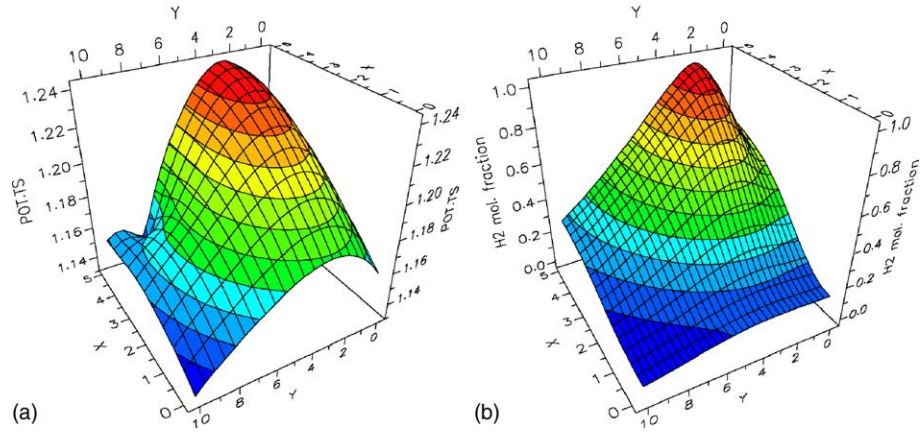

Fig. 2. Model outputs, all cases @28 A total current and 70% fuel utilization. (a) Temperature solid adiabatic, maximum temperature 1240 K, (b) hydrogen mole fraction.

concentration close to the middle of the cell. The steep decrease in concentration near the inlet is due to the extremely high current density at the inlet.

For the temperature field (seen in Fig. 2(a)), the hot spot is located close to the fuel entrance as expected in a counter flow situation. As the air flux is low, the hot spot is between the two inlets and the general temperature profile is similar for adiabatic and non-adiabatic boundary conditions. The maximum temperature changes from 1240 to 1085 K when changing the boundary conditions from adiabatic to non-adiabatic.

4.4. Validity of the model and accuracy problems

The results presented are computed with a finite difference scheme and the accuracy of the results can be affected by the size of the mesh used. This is specially the case here where a rather coarse mesh is currently used (with 200–1500 nodes on the surface).

Fig. 3(a) shows how the results on the temperature profile can be affected. The mesh size was varied from 11 × 21 to 31 × 61 to study the sensitivity of the results. As expected, the coarser mesh has a maximum temperature higher than the finer one (of ca. 25 K). Nevertheless, the shape of the temperature profile remains the same. It can be pointed out that for the two finer meshes, the temperature profile is similar.

The error on the species balance decreases with increasing mesh size from 1.2% on the coarser to less than 0.3% as reported in Table 2. The error seems to be related to the mesh definition. As the change in intensity and direction of velocity are very steep close to the inlet, most of the error may come from the inlet region. Ideally, the mesh should be refined near the inlet but this is unfortunately not possible with the tool used.

In order to use the model for optimization of decision variables, the important point is to verify that the mesh size has no impact on the sensitivity of the chosen criteria. For optimization, two objective functions are considered: maximizing the specific power output per unit volume in W/cm^3 and minimizing the maximum temperature of the solid. In Fig. 3(b), the sensitivity to the interconnect thickness of those two criteria is shown for two different mesh sizes. The

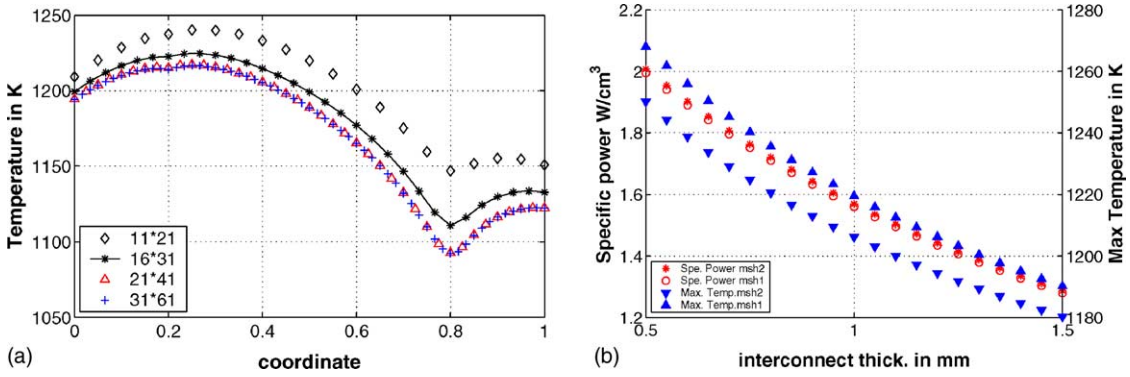

Fig. 3. Sensitivity to mesh size: temperature profile and response to a parameter change. (a) Temperature profile variation with increasing mesh size, @28 A total current, 70% f.u., adiabatic, the CPU time was 2, 15, 30 and 600 min. (b) Sensitivity to interconnect thickness for two different mesh sizes (mesh 1: 11 × 21, mesh 2: 16 × 31).

Table 2
Results sensitivity to the mesh size

	11 × 21	16 × 31	21 × 41	31 × 61	41 × 81	51 × 101
Error on species balance (%)	1.2	0.6	0.45	0.38	0.32	0.28
Maximum temperature solid (K)	1240.2	1224.5	1217.2	1216.6	–	–
Power output (W)	19.80	19.92	19.92	19.93	–	–

absolute value of the temperature differs by ca. 15 K but the response is perfectly similar. The model developed can therefore be used for optimization even with a coarse grid (which is required in term of CPU time).

5. Experimental validation

The developed model has been compared to experimental results for a repeat element. The performance is compared for three different operating conditions (in terms of hydrogen flux). The operating temperature was 1045 K (i.e. the environment temperature for the model) measured in the test oven.

5.1. IV characteristic validation

The results presented in Fig. 4 show simulated and measured IV curves for the three cases (@200, 300, 360 ml/min hydrogen flux and air ratio of 2.5). The cell was run up to 68–70% fuel utilization. The simulated data uses kinetic parameters identified on button cells (see Section 3.3). The model should then be able to simulate the performance of a repeat element using the same cells. The comparison of simulated and experimental characteristics shows that the response of the model to the flux is satisfactory, but that there is a large error on the open circuit voltage. The simulated open circuit voltage (OCV) is overestimated by ca. 100 mV.

The conclusion here is that the model used for simulation does not take into account a phenomena responsible for lower OCV. This lower OCV can be attributed to several phenomena: diffusion of species from the post-combustion area, leakage current [15] and problems on the sealing creating a cross-over of reactants.

In previous work, implementing diffusion from the post-combustion zone in a model for a cell based on electrolyte supported cells, good simulation of OCV depending on flux was obtained [2]. This aspect is implemented in the model (see Section 3.1) and contributes to a lowering of the OCV in the order of 20–40 mV compared to theoretical Nernst voltage. Leakage current has therefore to be added to the model.

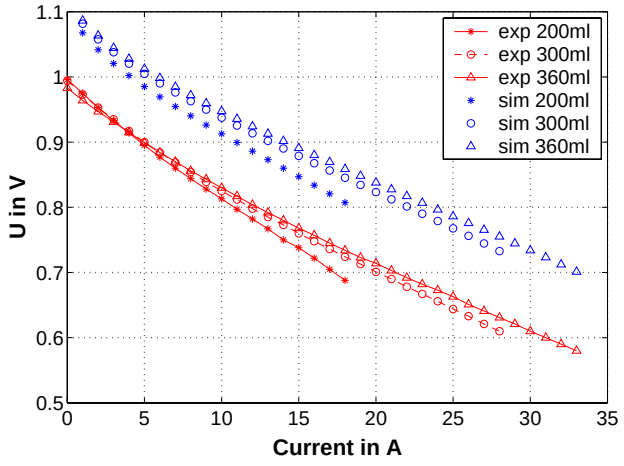

Fig. 4. Current potential (IV) characteristics: simulated and experimental; 52 cm^2, environment @1045 K, air ratio 2.5.

5.2. Leakage current model

At OCV, assuming the electrolyte is a pure ionic conductor, no consumption of species neither ionic current should be found. But if the electrolyte has some electronic conductivity, then it behaves like a mixed conductor and some ionic current exists even at OCV. When the cell is supplying current to a load, the external current is added to the internal short circuit current through the electrolyte. In anode supported cells, the electrolyte is very thin (6 μm in our case). From literature, the electronic resistance for this thickness is in the range of 5–100 Ω cm^2 [16–18].

The model chosen to represent the leakage current is based on the equivalent circuit shown in Fig. 5. At OCV the leakage current is essentially determined from the ionic and electronic resistance. The ionic resistance for the cell used in our experiment is assumed to be known [15], with a value of 0.12 Ω cm^2.

The equations describing the system are:

$$E_o - R_{ionic} j_{ion} - R_{tot} j_{load} = U_{cell} \quad (7)$$

$$j_{load} + j_{loss} = j_{ion} \quad (8)$$

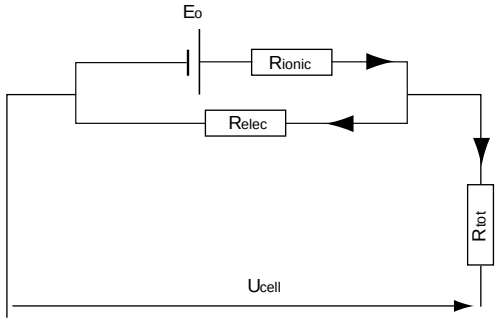

Fig. 5. Equivalent circuit for the electrode/electrolyte system.

Table 3
Cases for the OCV simulation comparison

Fluxes	Centered			Counter		
	Ce1	Ce2	Ce3	Co1	Co2	Co3
Fuel flow (ml/min)	180	230	260	250	300	400
Air flow (l/min)	2	2	2	2.3	2.5	2.5

where E_o is the local Nernst voltage; R_{ionic} is the ionic resistance of the electrolyte; j_{ion} is the ionic current through the electrolyte; R_{tot} is the resistance of the electrodes and interconnects; j_{load} is the current density in the electrodes; U_{cell} is the cell operating voltage.

At OCV, the current in the external circuit is zero and therefore the loss current can be computed at OCV as:

$$j_{loss} = \frac{E_o}{R_{ionic} + R_{elec}} \quad (9)$$

where R_{elec} is the electronic resistance of the electrolyte. For any operating point, the local loss current is described by the equation:

$$R_{elec} j_{loss} = U_{cell} + R_{tot} j_{load} \quad (10)$$

The value of the electronic resistance has to be estimated. Parameter identification method has been used to find the estimate. The experimental data used for the parameter estimation comes from three different experiments:

- a button cell of 16 cm^2 area with central feed [13]
- a repeat element with central feed of air and fuel on a square cell (80 mm side)
- a regular repeat element with improved sealing (compared to the IV curve experiment).

For these three experiments, three sets of conditions were available (see in Table 3). The identification has been performed on the three experiments with a common assumption that the electrolyte thickness was of 6 μm (the thickness has not been measured). The result from the parameter estimation is a value of 9.58 Ω cm^2 for the electrolyte electronic resistance. The 95% confidence interval is quite large with a range of ±2 Ω cm^2, the poor statistical quality of the result is due to a lack of data.

The comparison of the OCV on the two different repeat element configurations is presented in Fig. 6. The application of the leakage current model and the parameter optimization allow a sensible improvement of the OCV simulation. The remaining error is below 20 mV. The quality of the model could be improved with further experiments and parameter identification.

5.3. New simulation of the IV curve

The model for OCV calculation has then been applied to simulate the IV characteristics. With the identified value, an offset of ca. 40–50 mV remains. This could be explained by the fact that some reactants cross-over occurs in this repeat element (as the experimental OCV does not increase with the flux in this case) or to a slightly lower electrolyte thickness. Correcting the electrolyte thickness to 4.5 μm in the model inputs, the remaining error is of ca. 20 mV as shown in Fig. 7, which is satisfactory.

This last result shows that comparison of experimental data with simulation is essential to improve models. In this case, the error in OCV has necessitated to add a new phenomenon into the model and the order of magnitude of this phenomenon has been identified.

From the identified values for the electronic conductivity, the leakage current is in the order of 0.1 A/cm^2 which is not negligible at all. This affects the species balance as the leakage current involves conversion of hydrogen, therefore the effective fuel utilization is higher than the fuel utilization computed from the current drawn in the external circuit. This is particularly important and critical at high fuel utilization. When operating at 70% fuel utilization, the conditions in the cell are equivalent to operation at 75 or 80%. The leakage current may therefore limit the efficiency of the stack by limiting operation at high fuel utilization.

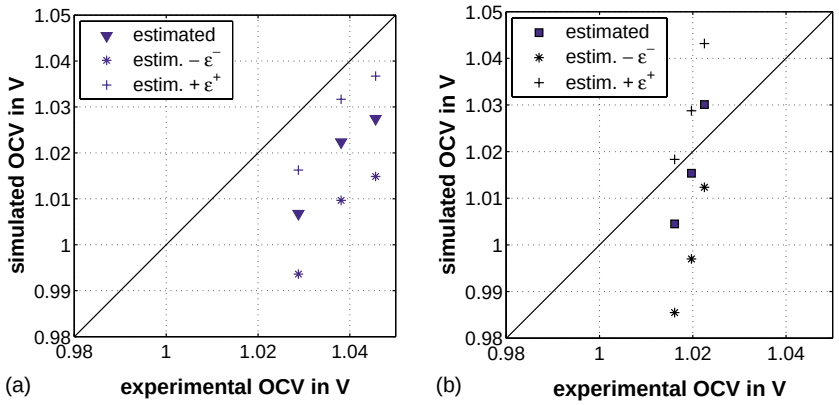

Fig. 6. Experimental vs. simulated OCV with estimated value for R_{elec}, filled sign are the estimated value, stars and cross gives simulation results with the lower and higher bound of the 95% confidence interval. (a) Central feed repeat element, (b) "counter" flow repeat element.

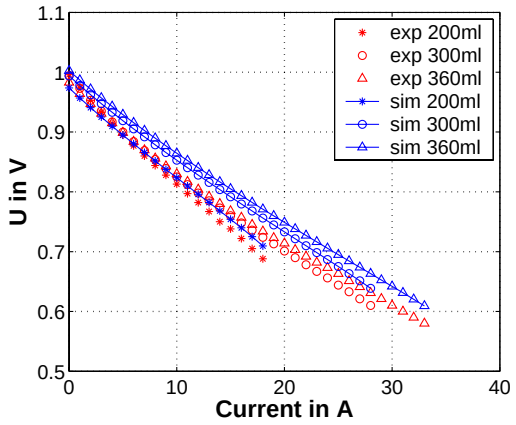

Fig. 7. Current potential (IV) characteristics: simulated (with leakage current model) and experimental; 52 cm^2, environment @1045 K, air ratio 2.5.

6. Comparison of configurations

The counter flow configuration (in Fig. 1(c)) is the first one to be experimentally demonstrated so far, but other configurations are possible based on the internal manifolding concept. The example shown next is described in Fig. 1(d). It uses a central feed for the fuel and two inlets for the air flow, the flow pattern being closer to a co-flow. To compare the results for this configuration with the counter flow case, simulations have been performed with the same cell size, same thickness for the interconnect, the same channel height and operating conditions (fluxes and temperature). The electrochemical characteristic is compared in parallel to the maximum temperature.

Fig. 8 shows the electrochemical performance to be quite similar for both cases. The maximum temperature encountered in the solid is quite different. The temperature is much higher in the counter flow configuration. This can be explained by the post-combustion that occurs only on one side for the counter flow case. The intensity of the heat release is then much higher than in the other case as the post-combustion takes place on the whole perimeter of the cell.

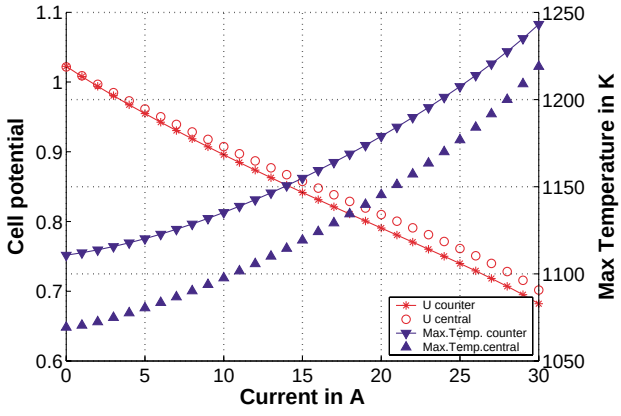

Fig. 8. Configuration comparison between “counter” flow and central feed.

A change in configuration can thus be an interesting solution to achieve a similar power output with lower temperature levels. A limit to the actual description of the flow field can be found with this case. To be effectively realized, sealing rings will have to be introduced, changing the flow pattern in the fuel side, this change is here significant as the fluid path is short. This may cause an overestimation of the electrochemical performance of such a cell.

7. Conclusion

The developed modeling tool has demonstrated ability to predict experimental results for the electrochemical performance of technical repeat element, to carry out sensitivity studies, and to be adapted to simulate new configurations. Therefore, in the present status this tool can be used to optimize repeat element and explore new configurations.

Experimental validation of the temperature field and on further experiments is expected to enhance the model and confidence on the results. Comparison of the results for the same case in a CFD model will be carried out. CFD may be used as well to verify the range of validity of some assumptions.

Boundary conditions definition needs to be further studied: adiabatic boundary conditions are the worst case scenario, not expected to be found in stack with metallic interconnects of less than 30 cells. This will have to be verified by using this repeat element model as a base for a stack model. Then, the results from this stack model will have to be used to define more realistic boundary conditions. The model will be extended to hydrocarbon reformed fuels which are planned be tested soon experimentally. Finally, further experiments are necessary to verify the preliminary results obtained for the leakage current.

As the simulation of an operating point can be quite fast, this model will be coupled to a multi-objective optimization algorithm to explore the range of possible solutions for each configuration and identify the interesting solutions. The tool presented here will be used in parallel to other models with different levels of details (with CFD) and different scales (stack model and system model) to form a conception and design platform for SOFC planar repeat element and stacks.

Acknowledgements

The Swiss Federal Energy Office (project 46795/contract 86895) and the Swiss Commission for Technology and Innovation (CTI project 5041.2SUS) are gratefully thanked for financial support. Thanks are due to Michele Molinelli for repeat element testing, and to HTceramix S.A. for cell and stack manufacturing.

References

[1] E. Achenbach, Three-dimensional and time-dependent simulation of a planar solid oxide fuel cell stack, J. Power Sources 49 (1994) 333–348.

[2] P. Costamagna, K. Honegger, Modeling of solid oxide heat exchanger integrated stacks and simulation at high fuel utilization, J. Electrochem. Soc. 145-11 (1998) 3995–4007.

[3] H. Yakabe, T. Ogiwara, I. Yasuda, 3D model calculation for the planar SOFC using multi-channel and stack models, in: Electrochemical Society (Ed.), Proceeding of the Seventh SOFC Conference, vol. 2001-16, 2001, pp. 1087–1098.

[4] B. Todd, J.B. Young, Thermodynamic and transport properties of gases for use in solid oxide fuel cell modelling, J. Power Sources 110 (2002) 186–200.

[5] P. Costamagna, The benefit of solid oxide fuel cells with integrated air pre-heater, J. Power Sources 69 (1997) 1–9.

[6] M. Roos, E. Batawi, U. Harnisch, Th. Hocker, On the systematic optimzation of ethanol fed SOFC-based electricity generating systems in terms of energy and exergy, J. Power Sources 114 (2003) 203–212.

[7] H. Karoliussen, K. Nisansioglu, A. Solheim, Use of effective conductivities and unit cell-based supraelements in the numerical simulation of solid oxide fuel cell stacks, J. Appl. Electrochem. 28 (1998) 283–288.

[8] F.P. Incropera, D.P. De Witt, Fundamentals of Heat and Mass Transfer, John Wiley and Sons, 1990.

[9] M. Oh, C. Pantelides, A modelling and simulation language for combined lumped and distributed parameters systems, Comput. Chem. Eng. 20-6/7 (1996) 611–633.

[10] D. Larrain, J. Van herle, M. Graetzel, D. Favrat, Modeling of cross-flow stack: sensitivity to thermal properties of the materials, in: Electrochemical Society (Ed.), Proceeding of the Eighth SOFC International Symposium, vol. PV 2003-07, 2003, pp. 1478–1486.

[11] T. Kawashima, M. Hishinuma, Thermal properties of porous Ni/YSZ particulate composites at high temperatures, Mater. Trans. JIM 37-9 (1996) 1518–1524.

[12] U. Bossel, Final Report on SOFC Data -Facts and Figures, International Energy Agency SOFC Task Report, Bern, April 1992.

[13] D. Larrain, J. Van herle, F. Maréchal, D. Favrat, Thermal modeling of a small anode supported solid oxide fuel cell, J. Power Sources 114 (2003) 203–212.

[14] M. Molinelli, D. Larrain, R. Ihringer, L. Constantin, N. Autissier, O. Bucheli, D. Favrat, J. Van herle, Current collection and stacking of anode supported cells with metal interconnects to compact repeating units, in: Electrochemical Society (Ed.), Proceeding of the Eighth SOFC International Symposium, vol. PV 2003-07, 2003, pp. 203–212.

[15] R. Ihringer, Electrolytes minces sur supports anode dans les piles à combustible SOFC. Ph.D. thesis, Swiss Federal Institute of Technology of Lausanne, 2001 (number 2307).

[16] K. Kobayashi, S. Yamaguchi, T. Higuchi, S. Shin, Y. Igushi, Electronic transport properties and electronic structure of TiO_2-doped YSZ, Solid State Ionics 1–4 (135) (2000) 643–651.

[17] T. Kawada, H. Sakai, H. Yokokawa, M. Dokiya, Electrical properties of transition-metal-doped YSZ, Solid State Ionics 53–56 (1992) 418–425.

[18] A.V. Virkar, Theoritical analysis of solid oxide fuel cells with two-layer, composite electrolytes: electrolyte stability, J. Electrochem. Soc. 138 (5) (1991).